Hot spot activity and tectonic settings near Amsterdam-St. Paul plateau (Indian Ocean)

Myriam Janin, Christophe C Hémond, Hervé Guillou, Marcia Maia, M. K. T. Johnson, Claire Bollinger, Céline C. Liorzou, A. Mudholkar

Hot spot activity and tectonic settings near Amsterdam–St. Paul plateau (Indian Ocean)

M. Janin,[1,2] C. Hémond,[1,2] H. Guillou,[3] M. Maia,[1,2] K. T. M. Johnson,[4] C. Bollinger,[1,2] C. Liorzou,[1,2] and A. Mudholkar[5]

Received 22 June 2010; revised 14 February 2011; accepted 25 February 2011; published 20 May 2011.

[1] The Amsterdam–St. Paul (ASP) plateau is located in the central part of the Indian Ocean and results from the interaction between the ASP hot spot and the Southeast Indian Ridge (SEIR). It is located near the diffuse boundary between the Capricorn and Australian plates. The seamount chain of the Dead Poets (CDP) is northeast of the ASP plateau and may represent older volcanism related to the ASP hot spot; this chain consists of two groups of seamounts: (1) large flat-topped seamounts formed 8–10 Ma and (2) smaller conical seamounts formed during the last 2 Myr. The ASP hot spot has produced two pulses of magmatism that have been ponded under the ASP plateau and erupted along the divergent boundary between the Capricorn and Australian plates. The N65° orientation of the CDP as well as the seamount's elongated shapes support an opening motion between the Capricorn and Australian plates along a suture oriented in the N155° direction. This motion compared to the Antarctic plate amounts to an apparent velocity of 7.7 cm/yr northeastward for the Capricorn-Australian block. This motion does not fit with a fixed plume model. We suggest, therefore, that the ASP plume experienced a motion of about 1–2 cm/yr to the SW, which is opposite to the asthenospheric flow in this region and suggests a deep-seated plume.

Citation: Janin, M., C. Hémond, H. Guillou, M. Maia, K. T. M. Johnson, C. Bollinger, C. Liorzou, and A. Mudholkar (2011), Hot spot activity and tectonic settings near Amsterdam–St. Paul plateau (Indian Ocean), *J. Geophys. Res.*, *116*, B05206, doi:10.1029/2010JB007800.

1. Introduction

[2] Interaction between ridges and hot spots occur in all oceans and in various geodynamic contexts. When a ridge is located directly above a plume the excess heat results in enhanced melting and magma production [*Schilling*, 1973; *Vogt*, 1976]. One of the main consequences is the construction of large oceanic plateaus, such as the Icelandic and Azores plateaus [*Schilling*, 1991; *Gente et al.*, 2003]. In the Indian Ocean, the Southeast Indian ridge (SEIR) has interacted with two hot spots over the last 40 Myr, which resulted in the construction of two oceanic plateaus: (1) the northern Kerguelen plateau, which started to form about 40 My ago [*Frey et al.*, 2000], and (2) the Amsterdam–St. Paul plateau, which has been active over the last 10 My [*Maia et al.*, 2008].

[3] The construction of these oceanic plateaus has been complicated by the fact that the history of plate motion in the Indian Ocean is complex. Three main diverging plates induced the formation of three spreading ridges: the Central Indian Ridge (CIR hereafter) between the African and Indo-Australian plates, the Southwest Indian Ridge (SWIR) between the African and Antarctic plates, and the Southeast Indian Ridge (SEIR) between the Indo-Australian and Antarctic plates. However, the plate motion in the Indian Ocean is inconsistent with a rigid Indo-Australian plate model [*Minster and Jordan*, 1978; *Stein and Gordon*, 1984; *Demets et al.*, 1988] and more likely is the result of the interaction between four distinct subplates (Indian, Capricorn, Australian, and Macquarie) separated by diffuse boundaries [*Minster and Jordan*, 1978; *Wiens et al.*, 1985; *Demets et al.*, 1988; *Royer and Gordon*, 1997] (Figure 1). The Capricorn and Australian plates are divergent near the CIR and SEIR and their diffuse boundary seems to accommodate the resulting deformations. The actual boundary between the Capricorn and Australian plates intersects the SEIR near the St. Paul fracture zone (SPFZ) [*Conder and Forsyth*, 2001].

[4] The Amsterdam–St. Paul (ASP)/SEIR interaction system successively underwent the three possible geometries for the interaction of a ridge and a hot spot, that is to say the ridge approaches, overlies, and finally moves away from the plume. This makes it of special interest for the study of

[1]Université Européenne de Bretagne, Brest, France.
[2]Domaines Océaniques, UMR 6538, Université de Brest, CNRS, Institut Universitaire Européen de la Mer, Plouzané, France.
[3]LSCE/IPSL, Laboratoire CEA-CNRS-UVSQ Domaine, CNRS, Gif sur Yvette, France.
[4]School of Ocean and Earth Science and Technology, University of Hawaii, Honolulu, Hawaii, USA.
[5]National Institute of Oceanography, Goa, India.

0148-0227/11/2010JB007800

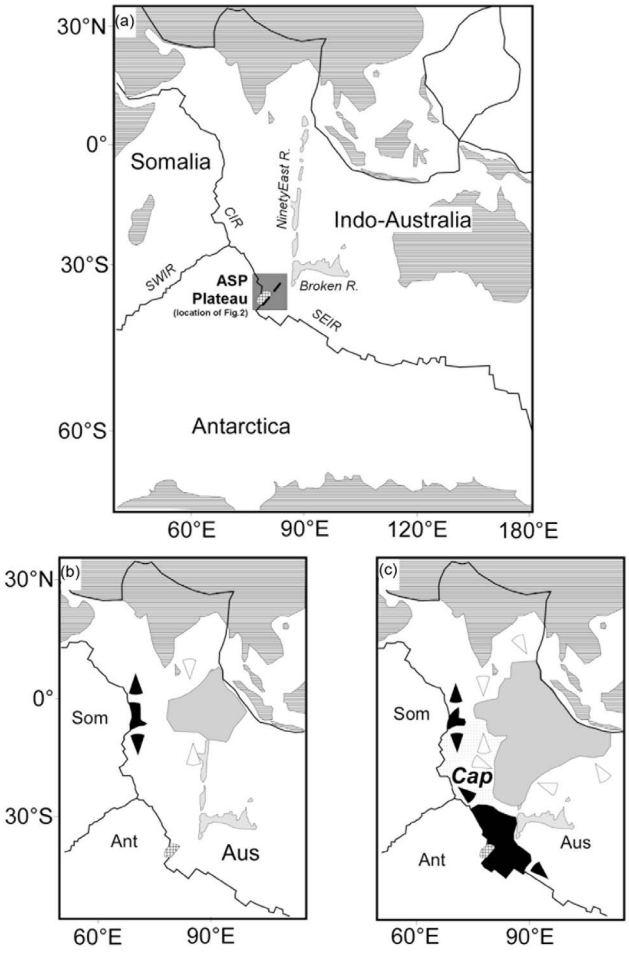

Figure 1. Tectonic settings and assumptions (modified from *Royer and Gordon* [1997] with permission from AAAS). (a) Traditional Indo-Australian plate boundaries. R, ridge; CIR, Central Indian Ridge; SWIR, Southwest Indian Ridge; SEIR, Southeast Indian Ridge. (b) Plate boundaries and tectonic stresses as proposed by *Demets et al.* [1994]. Som, Somalian plate; Ant, Antarctic plate; Aus, Australian plate. (c) Plate boundaries and tectonic stresses as proposed by *Royer and Gordon* [1997] with the addition of the Capricorn plate (Cap). The Macquarie plate is located easternward (140° to 160°E) and is thus not present. In Figures 1b and 1c, black area, with converging black triangles, denotes diffuse boundaries accommodating horizontal divergence, and gray area, with diverging open triangles, denotes diffuse boundaries accommodating horizontal convergence.

ridge–hot spot interactions. In addition, the proximity of Capricorn/Australian plate boundary may also have influenced the local volcanism and the construction of the plateau. This area was the target of the MD157/PLURIEL cruise (N/O Marion Dufresne, September/October 2006). This cruise was dedicated to map and sample the ASP plateau and the Chain of the "Dead Poets" (CDP) (Figure 2). Preliminary geophysical results obtained during the cruise have been presented elsewhere [*Maia et al.*, 2008] and a detailed analysis of the surface magnetism, the gravity and the bathymetry is presented in two companion papers (M. Maia et al., Building of the Amsterdam–St. Paul plateau: A 10 Myr history of a ridge–hot spot interaction and variations in the strength of the hot spot source, submitted to *Journal of Geophysical Research*, 2011; E. Courreges et al., Evolution of ridge segmentation on the St. Paul–Amsterdam plateau from 10 Ma, in the context of ridge–hot spot interaction, submitted to *Journal of Geophysical Research*, 2011). This work presents a geochronological reconstruction of the volcanic features related to ASP hot spot prior and during its interaction with the SEIR.

2. Geological Setting

2.1. Context of the Study

[5] The ASP plateau is a complex structure and the result of several processes. It is limited by the Amsterdam fracture zone (AFZ) toward the northwest, the St. Paul fracture zone (SPFZ) toward the southeast and is crosscut by the SEIR (Figure 2). This plateau is mostly submarine with only two subaerial features, the Amsterdam and St. Paul islands. They are located 80 km apart and are younger than 0.4 Ma [*Watkins et al.*, 1975]. Their isotope compositions clearly indicate that they derive from a mantle plume distinct from the Kerguelen hot spot [*Doucet et al.*, 2004]. Recently, the Boomerang expedition Leg 9, on the SEIR between 77 and 88°E (R/V Melville, 1996), discovered a small active seamount on the ASP plateau, near the SEIR Segment I (following the names of *Royer and Schlich* [1988]) [*Johnson et al.*, 2000]. This cruise collected dredge samples and published a complete geochemical study of SEIR Segments I and J that currently are crossing the ASP plateau [*Nicolaysen et al.*, 2007]. This work suggests a heterogeneous source at a rather small scale, but their limited geographical coverage does not allow a representative picture of the whole geodynamic evolution of the ASP plateau to be developed.

[6] The ASP plume, presently located beneath Amsterdam and St. Paul islands, was originally located beneath the Australian Plate. The interaction phase with the SEIR and the construction of the ASP plateau began about 10 Ma ago [*Maia et al.*, 2008]. Observed magnetic anomalies (see Figure 3) exhibit a multistage history with two ridge jumps of the SEIR at 6.3 and 3.3 Ma (E. Courreges et al., submitted manuscript, 2011). Maia et al. evaluated the crustal structure of the plateau using the calculated positions of the plume in the past and the rheology of the lithosphere, leading them to conclude that plume flux varied during construction of the plateau. Changes of its relative position to the SEIR could also account for the morphology changes and hence related magma flux variations. In other words, there were two periods of higher melt supply between 9.7 and 6.3 Ma and between 3.3 and 0.9 Ma, separated by a lower magmatic production stage. The on-axis major magmatic stage, responsible for the construction of the plateau is represented by three samples in our sample suite: PLU DR 6-1-1, PLU DR 6-2-2, and PLU DR 34-1-1. The northeastern part of the plateau, located on the Australian plate, contains a short volcanic chain of seamounts, which show a variety of morphologies from small volcanoes (PLU DR 10-1-1, PLU DR 10-2-2) to large seamounts (PLU DR 39-1-1/Rimbaud). They are either built on to the plateau or on its edge and represent a later off-axis magmatic stage. The difference

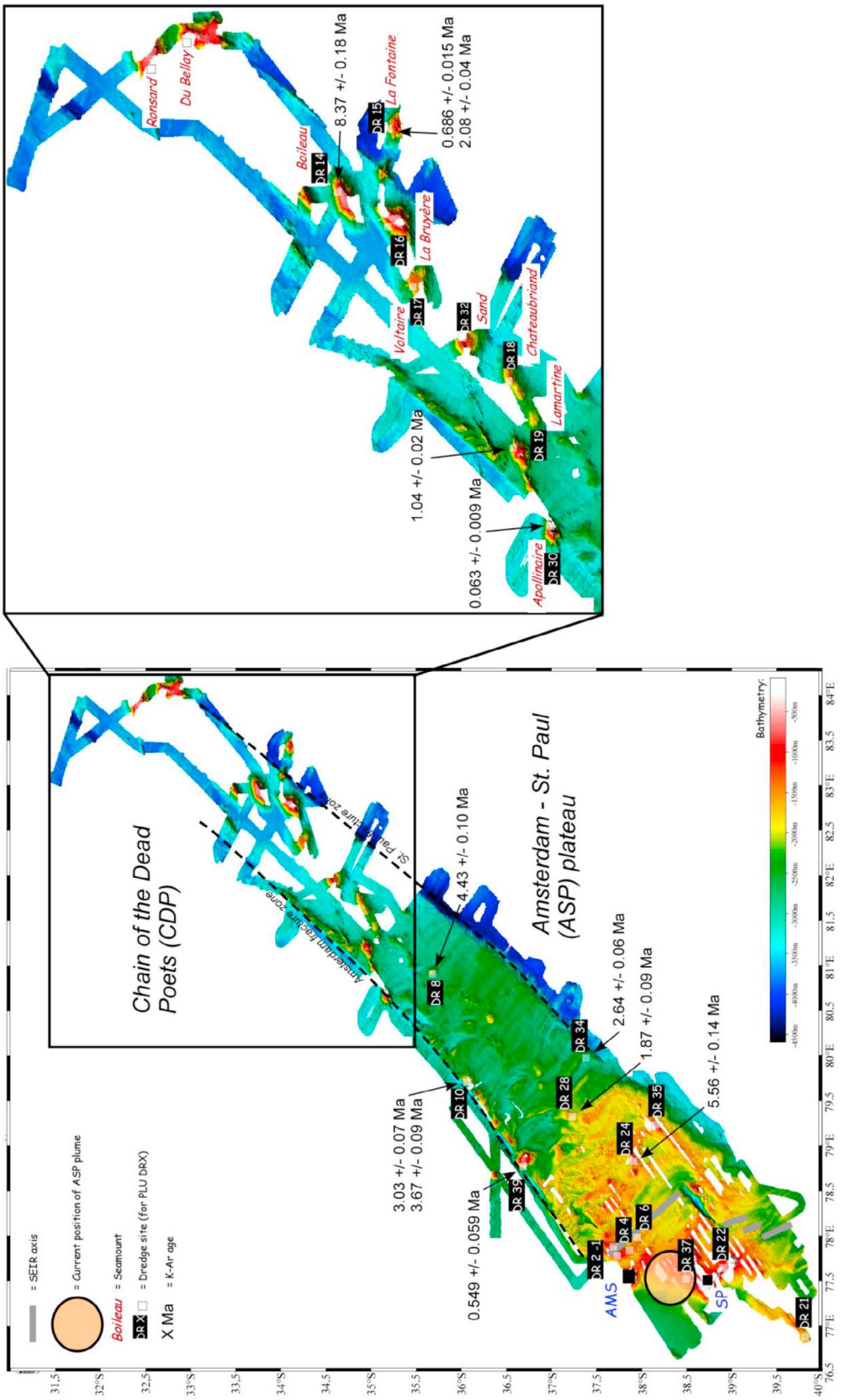

Figure 2. Bathymetry of ASP plateau with a focus on the chain of Dead Poets mapped during the MD157/PLURIEL cruise. White square (in transparency) represents basalts samples with the related dredge (PLU DR) number. On the chain of Dead Poets the name of the seamounts are noted. Two seamounts are named without dredge number because no basalt samples were available. Black squares are the localization of Amsterdam (AMS) and St. Paul (SP) islands. Dotted lines are the fracture zones limiting ASP plateau. K-Ar datings of the edifices are reported on the map.

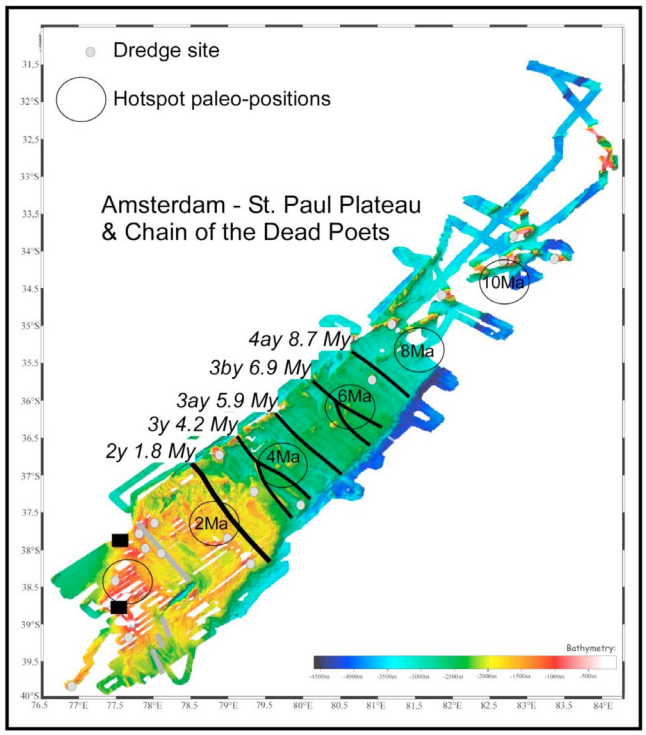

Figure 3. Interpreted magnetic anomalies (black lines) from E. Courreges et al. (submitted manuscript, 2011) plotted on ASP plateau and chain of Dead Poets bathymetry. The corresponding chrons (2 y to 4 ay with their corresponding age) are from *Cande and Kent* [1995]. Empty circle is the modeled paleopositions of the hot spot (M. Maia et al., submitted manuscript, 2011) every 2 My (from the supposed current position between Amsterdam and St. Paul islands until the 10 My paleoposition). Dredge sites are represented for information.

between on- and off-axis magmatism is thus highlighted by the structure morphology with (1) on-axis magmatism building a thicker oceanic crust and (2) off-axis magmatism occurring later and resulting into the construction of edifices on the oceanic bottom.

[7] In this paper, we used K-Ar dating to constrain the ASP hot spot activity. We also used morphological features and some geochemical characteristics to further group events when geochronology data could not be used. It helped also to depict the influence of tectonic stresses during the construction of the ASP plateau and seamounts.

2.2. Structures and Samples Description

[8] The modeled track of the ASP hot spot, which may represent the ASP plume activity prior its interaction with the SEIR, is parallel to the chain of seamounts located between 80°E 30′ and 87°E, between the ASP and the Broken Ridge plateaus [*Luyendyk and Rennick*, 1977; *Royer and Schlich*, 1988]. This work will focus on the part of the chain located between 80°30E and 84°E (Figure 2). However, it is important to note that there is no evidence of an oceanic plateau at the beginning of the supposed ASP hot spot track; that is, the initial plume activity does not reflect the impact of a plume head. From SW to NE, eight seamounts were identified: Apollinaire; Lamartine, Chateaubriand, Sand, Voltaire, La Bruyère, Boileau, and La Fontaine. Together with the Ronsard and Du Bellay seamounts, located northward, they constitute the chain of the Dead Poets (CDP). The last two seamounts are not considered in this paper because of very incomplete bathymetric data and lack of fresh rock samples for geochemical analyses and age dating. Some morphological characteristics are summarized in Table 1. The CDP is composed of two types of seamounts: those with steep summits and those with flat summits as seen in cross section (Figure 4). Special attention has to be paid to Lamartine as its cross section suggests a flat summit, but the digital elevation model (DEM) reveals that this seamount is composed of two distinct sharp summits.

[9] Boileau and La Bruyère seamounts are special since they are the only two with a basal area greater than 800 km^2 while all the other seamounts are smaller than 500 km^2. This means that their volume is about 2 to 4 times greater, which combined with their flat summit profiles could indicate that those seamounts were above sea level for some time, forming a volcanic island and then getting eroded and submerged again.

[10] The morphology of the seamounts appears to be elongated with a length/width ratio larger than 1.4 for all but La Fontaine seamount. Both the chain and the long axis of the seamounts show a N65° orientation. This orientation, different from the SEIR N50° spreading direction, suggests at least a partial tectonic control on the seamount construction. All the samples collected during the PLURIEL cruise and used in this study are presented in the Table 2. The CDP samples are highly alkaline, reaching the tephrite/basanite compositions (Figure 5 TAS diagram [*Le Bas et al.*, 1992]). In contrast, the plateau samples are mostly tholeiitic basalts except for the current SEIR samples, which are andesitic basalts. We report unpublished data from PLURIEL samples not used in this geochronological paper for comparison. Petrographically the CDP samples are richer in vesicles than the plateau samples but we have not noted any petrographic systematic variation with the location or the depth of the collected samples.

3. K-Ar Geochronology

3.1. Procedure

3.1.1. Selection and Preparation of the Samples

[11] Eighteen samples were selected for geochronological study based on their distance from the ridge axis and their degree of alteration. Glassy samples were avoided because of possible excess argon caused by rapid quenching which impedes loss of the noninitial atmospheric argon [*Dalrymple and Lanphere*, 1968]. Major elements analyses were used to estimate the degree of alteration of the samples and to establish the rock type of the samples (Table 3). The K_2O versus Nb ratio is a good indicator of alteration, whereby alteration would cause increases in K_2O for any given Nb value (Figure 6). The K_2O and Nb values measured on whole rocks samples are reported in Table 3. The good correlation between K_2O and Nb (R^2 = 0.983), and the generally (moderately) low LOI values, confirms that the samples have not undergone significant post magmatic alteration. The loss on ignition value (LOI) of these samples range from 0.01 to 1.11% with an extreme sample with

Table 1. Morphologic Characteristics of the Chain of Dead Poets Seamounts From SW to NE Locations

Seamount	Length, L (km)/Width, W (km)	Height (km)	Base Area (km^2)	Summit	Orientation (N°)
Apollinaire (PLU DR30)	L = 24/W = 16	2.7	325		65
Lamartine (PLU DR19)	L = 23/W = 16	2.1	280		65
Chateaubriand (PLU DR 18)	L = 36/W = 21	1.9	580		65
Sand (PLU DR32)	L = 35/W = 25	2.5	490		65
Voltaire (PLU DR17)	L = 30/W = 18	1.8	400		60
La Bruyère (PLU DR16)	L = 40/W = 27	3.3	800	flat	55
Boileau (PLU DR14)	L = 42/W = 24	2.9	900	flat	70
La Fontaine (PLU DR15)	L = 27/W = 26	2.9	470		90

3.44%. On the basis of its LOI sample, PLU DR14-1-1 could be considered altered but the LOI measurements were performed on the whole rock whereas K-Ar experiments were conducted on the cleaned groundmass. As detailed below alteration phases were removed mechanically and chemically. Since alteration phases on this sample were clearly aggregated in a small area, we are very confident in the separation of a cleaned groundmass.

[12] After macroscopic and microscopic inspections, groundmass aliquots from fresh samples were prepared following the procedure described by *Guillou et al.* [1998]. The excess $^{40}Ar^*$ component can be partially avoided when processing only the well-crystallized interiors of submarine basalt flows [*Dalrymple and Lanphere*, 1968; *Duncan and Hogan*, 1994]. All our samples were taken as far as possible (at least 4 cm) from the glassy rims of the pillows. The groundmass is assumed to have formed shortly after eruption and should not contain any excess $^{40}Ar^*$. All the samples were crushed and sieved to 0.250–0.125 mm size fractions and ultrasonically washed in acetic acid (1N) for 45 min at a temperature of 60°C, to remove any secondary minerals phase that might be present in minute amounts.

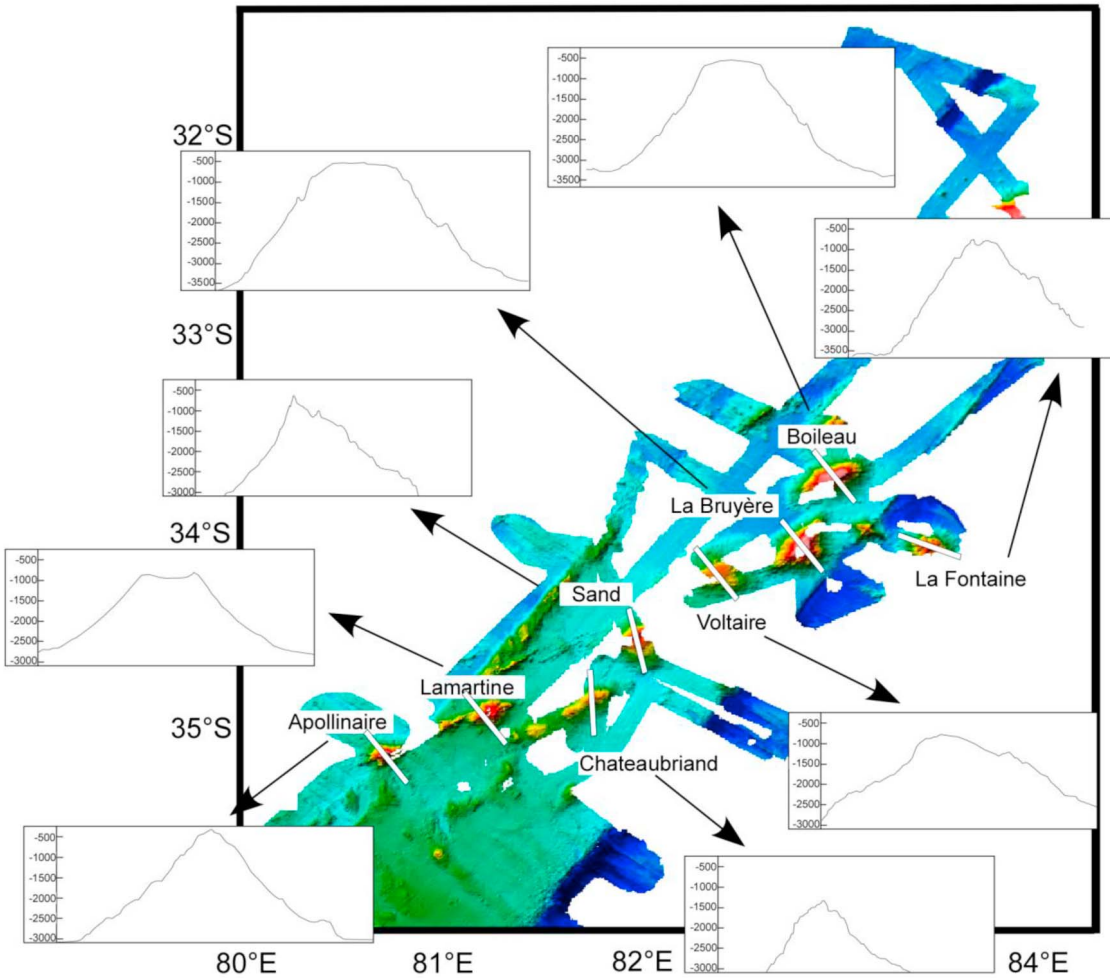

Figure 4. Morphologic profile of each seamount. White rectangles denote the location of cross sections on the chain of Dead Poets bathymetry. The vertical scale is similar for all the seamounts.

Table 2. Localizations and Descriptions of PLURIEL Cruise Dredges[a]

Dredge Number and Name	Latitude	Longitude	Depth (m)	Site	Dredge Description	Sample Used in This Study	Sample Macroscopic Description	Sample Petrography
PLU DR1 Boomerang	S37°41.50; S37°40.53	E77°54.90; E77°53.91	910; 760	Seamount	Mostly pillow lavas ; some with glass Volcanic brechia with sediments	PLU DR1-2-5	Fragment of vesicular pillow lavas	Phenocrysts : −; Microcrysts : Ol+Pl; Vesicles : ++; TAS : tholeiitic basalt
PLU DR2	S37°35.68; S37°35.67	E78°00.99; E78.00.40	1030; 1010	Seamount	Only pillow lavas but different types (glassy, vesicular, aphyric and/or, sedimentary rim	PLU DR 2-1-1	Fragment of pillow lavas with fresh glass	Phenocrysts : −; Microcrysts : Ol+Pl; Vesicles : ++; TAS : tholeiitic basalt
PLU DR3	S37°38.90; S37°39.10	E78°09.00; E78°08.02	2025; 2040	Oceanic floor	Empty			
PLU DR4	S37°51.50; S37°51.80	E78°03.50; E78°03.00	1900; 1800	Oeanic floor	Only pillow lavas	PLU DR4-1-3	Fragment of vesicular and aphyric pillow lavas with a small amount of glass	Phenocrysts : −; Microcrysts : Ol+Pl; Vesicles : +; TAS : tholeiitic basalt
						PLU DR4-1-5	Fragment of vesicular and aphyric pillow lavas without glass	Phenocrysts : −; Microcrysts : Ol+Pl; Vesicles : +; TAS : tholeiitic basalt
PLU DR5	S38°00.20; S38°00.21	E77°45.58; E77°44.66	905; 690	Seamount	Mostly carbonate soil with lavas and glass fragment. A lot of biological organism such as coral and urchin			
PLU DR6	S38°04.18; S38°04.08	E78°13.79; E78°12.23	1795; 1750	SEIR axis	Blocks of fresh basalt (pillows and tubes) with a large amount of glass	PLU DR6-1-1	Fragment of lava tube with glassy rim	Phenocrysts : −; Microcrysts : Ol+Pl+Px; Vesicles : +; TAS : andesitic basalt
PLU DR7	S36°19.00; S36°19.00	E80°25.85; E80°25.30	2000; 1860	Seamount	Manganese debris			
PLU DR8	S35°39.75; S35°40.70	E80°55.70; E80°55.10	2000; 1670	Seamount	Pillow lavas with sediments	PLU DR8-1-1	Fragment of pillow lavas with a small amount of vesicles and Mn crust	Phenocrysts : −; Microcrysts : Pl+Px; Vesicles : ++; TAS : tholeiitic basalt
PLU DR9	Dredge lost	Dredge lost	Dredge lost					
PLU DR10	S36°03.79; S36°03.69	E79°43.77; E79°41.77	1800; 1520	Inside corner	Blocks and fragments of lava with manganese crust	PLU DR10-1-1	Pillow lava with some vesicles and phenocrysts	Phenocrysts : Ol; Microcrysts : Ol+Pl+Px; Vesicles : +; TAS : tholeiitic basalt
						PLU DR10-2-2	Pillow lava with more phenocrysts	Phenocrysts : Pl; Microcrysts : Ol+Pl+Px; Vesicles : −; TAS : tholeiitic basalt
PLU DR11	Dredge lost	Dredge lost	Dredge lost					
PLU DR12	S32°20.91; S32°21.36	E83°50.39; E83°49.40	2230; 2240	Seamount	Only sediments			
PLU DR13	S32°44.31; S32°44.24	E84°04.86; E84°04.67	1560; 1450	Seamount	Diversified dredge with fragments of altered basalt, hyaloclastites, manganese, biological organism and sediments			

Table 2. (continued)

Dredge Number and Name	Latitude	Longitude	Depth (m)	Site	Dredge Description	Sample Used in This Study	Sample Macroscopic Description	Sample Petrography
PLU DR14 Boileau	S33°40.51; S33°40.63	E83°04.52; E83°04.30	2520; 2440	Seamount	Fragments of lava with mangenese crust, sediments	PLU DR14-1-1	Fragments of lava with mangenese crust	Phenocrysts : −; Microcrysts : Ol+Pl+Px; Vesicles : ++; TAS : tephrite
PLU DR15 La Fontaine	S34°04.92; S34°05.64	E83°27.41; E83°27.87	1600; 1560	Seamount	Blocks and fragments of lava, sediment	PLU DR15-1-1	Fragment of vesicular lava	Phenocrysts : −; Microcrysts : Ol; Vesicles : ++; TAS : tephrite
						PLU DR 15-2-3	Idem with smaller vesicles	Phenocrysts : −; Microcrysts : Ol+Pl+Px; Vesicles : ++; TAS : tephrite
PLU DR16 La Bruyère	S34°03.90; S34°03.80	E82°42.70; E82°42.60	2200; 2200	Seamount	Blocks and fragments of lava, sediment			
PLU DR17	S34°18.89; S34°18.22	E82°24.70; E82°25.49	2140; 1980	Seamount	Fragment of altered lavas, brechia, manganese			
PLU DR18	S34°50.78; S34°51.55	E81°47.25; E81°46.34	2150; 1820	Seamount	1 block of altered lava			
PLU DR19 Lamartine	S34°55.48; S34°55.21	E81°16.46; E81°16.21	1820; 1440	Seamount	Numerous fragments of pillow lava and tubes. Some biological organism (coral and urchin), sediment	PLU DR19-2-2	Fragment of pillow lavas	Phenocrysts : −; Microcrysts : Ol+Pl; Vesicles : ++; TAS : tephrite
PLU DR20	S35°02.52; S35°03.99	E81°23.12; E81°22.28	2120; 1940	Seamount	Numerous fragments of pillow lava and brechia			
PLU DR21	S39°49.08; S39°48.71	E76°51.05; E76°50.70	1400; 1240	Seamount	Blocks and fragments of lava, sediment			
PLU DR22	S39°02.89; S39°02.09	E77°43.21; E77°43.25	980; 860	Seamount	Blocks and fragments of lava of diverse types (vesicular, aphyric, glassy). A lot of biological organism (fish, coral, urchin, shellfish, seaspider)	PLU DR22-4-1	Fresh vesicular lava	Phenocrysts : −; Microcrysts : Ol+Pl+Px; Vesicles : ++; TAS : alkaline basalt
PLU DR23	S38°40.06; S38°39.28	E77°40.45; E77°40.48	1160; 900	Seamount	Mostly coral and sediment, two fragment of vesicular basalt			
PLU DR24	S37°54.99; S37°54.18	E78°54.20; E78°50.70	1310; 900	Seamount	Only fragment of lava, some with glass	PLU DR24-1-1	Block with a small amount of vesicles and Mn crust	Phenocrysts : Pl; Microcrysts : Pl+Pl; Vesicles : +; TAS : andesitic basalt
PLU DR25	S37°37.21; S37°37.20	E78°37.63; E78°36.49	1160; 900	Seamount	Mostly carbonates, fragments of altered basalt			
PLU DR26	S37°30.93; S37°31.13	E78°54.51; E78°54.33	1710; 1660	Seamount	Empty			
PLU DR27	S37°31.71; S37°32.07	E78°55.91; E78°55.50	1830; 1660	Seamount	Three small fragments of basalt			

Table 2. (continued)

Dredge Number and Name	Latitude	Longitude	Depth (m)	Site	Dredge Description	Sample Used in This Study	Sample Macroscopic Description	Sample Petrography
PLU DR28	S37°22.71; S37°23.19	E79°16.23; E79°15.78	1430; 1350	Seamount	Fragments of massive lava, some with manganese crust, sediment and coral	PLU DR28-1-1	Massive lava with a lot of small vesicles	Phenocrysts : Ol+Pl; Microcrysts : Pl; Vesicles : +; TAS : tholeiitic basalt
PLU DR29	S36°10.28; S36°10.42	E80°34.37; E80°34.08	2050; 1810	Seamount	Fragments of lava			
PLU DR30 Apollinaire	S35°09.47; S39°09.95	E80°41.37; E80°41.37	1100; 820	Seamount	Blocks and fragments of lava of diverse types (vesicular and/or aphyric). A lot of biological organism (fish, coral, urchin, shellfish)	PLU DR 30-1-1	Fragment of aphyric and vesicular lavas	Phenocrysts : −; Microcrysts : Ol+Pl; Vesicles : ++; TAS : tephrite
PLU DR31	S34°22.67; S34°22.84	E81°30.25; E81°30.74	2300; 1920	Seamount	Hyalocalstites with altered basalt			
PLU DR32 Sand	S34°34.98; S34°35.12	E81°56.52; E81°56.66	1140; 1140	Seamount	Block of lavas			
PLU DR33	S36°18.20; S36°18.19	E81°17.05; E81°16.33	3990; 3600	fracture zone	Mostly sediments with some manganese nodule			
PLU DR34	S37°24.74; S37°24.75	E80°03.84; E80°03.54	3050; 2850	Oceanic floor	Fragments of pillow lavas, sediments	PLU 34-1-1	Fragment of pillow lava with some vesicles	Phenocrysts : Ol+Pl; Microcrysts : Ol+Pl; Vesicles : +; TAS : tholeiitic basalt
PLU DR35 Verlaine	S38°10.65; S38°10.80	E79°12.50; E79°11.70	1100; 860	Seamount	Fragments of pillow lavas, sediments and coral			
PLU DR36	S38°02.16; S38°02.24	E79°38.82; E79°39.04	3000; 2400	fracture zone	Only sediment			
PLU DR37	S38°22.72; S38°21.84	E77°41.20; E77°39.85	1080; 960	Seamount	Fragment of lavas, red sediment, biological organism (coral, starfish, shellfish)			
PLU DR38	S38°17.34; S38°18.97	E77°46.64; E77°46.76	1200; 1000	Seamount	Only sediment and biological organism (coral, shellfish)			
PLU DR39 Rimbaud	S36°44.19; S36°44.09	E78°55.23; E78°55.03	1470; 960	Seamount	Large amount of pillow lavas	PLU DR39-1-1	Fragment of aphyric pillow lava. Fresh aspect but a small Mn crust	Phenocrysts : −; Microcrysts : Ol+Pl; Vesicles :+; TAS : tholeiitic basalt
PLU DR40	S36°23.75; S36°23.17	E79°16.46; E79°15.87	1520; 1260	Seamount	Only sediment with fragment of manganese			

[a]The two mentioned positions are the beginning and end of dredging, respectively. The samples used in this study are specifically described (included their position in the TAS diagram (Figure 5)).

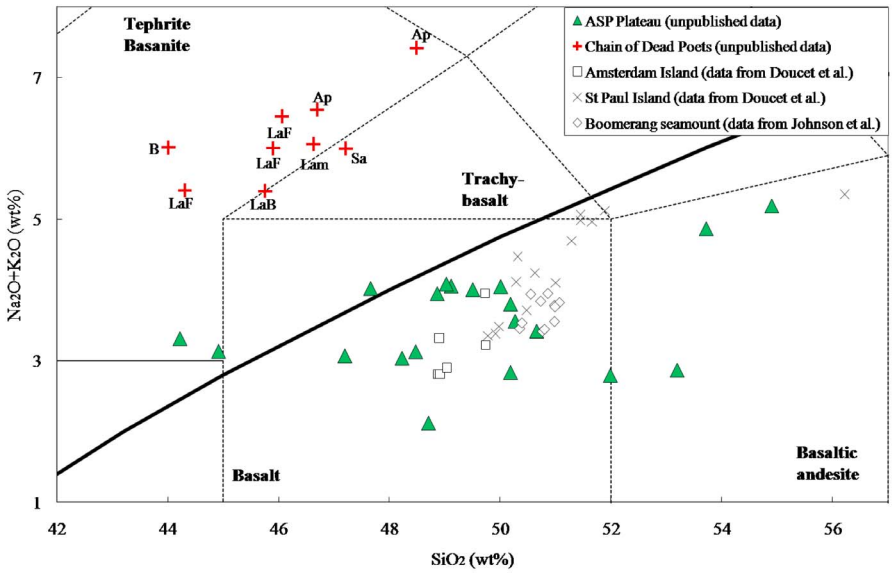

Figure 5. Total alkalis versus silica (all in wt %) diagram illustrating the range of petrological compositions for samples from the chain of Dead Poets and the ASP plateau. The fields used are from *Le Bas et al.* [1992]. The black line separates alkaline fields from tholeiitic fields. Data from *Johnson et al.* [2000] and *Doucet et al.* [2004] are plotted for comparison. Ap, Apollinaire; B, Boileau. LaB, La Bruyère; LaF, La Fontaine; Lam, Lamartine; Sa, sand.

Phenocrysts and xenocrysts, which are potential carriers of extraneous $^{40}Ar^*$ (including excess and inherited components), were eliminated using magnetic, gravimetric and visual hand-picking separation.

3.1.2. Measurement

[13] The unspiked K-Ar technique dynamically compares the isotopic composition of an aliquot of pure atmospheric Ar with the sample Ar composition to accurately determine minor variations of the $^{40}Ar/^{36}Ar$ isotopic ratio between the standard and the unknown. This method provides a precise correction for atmospheric Ar contamination and it avoids any discrimination effects of the mass spectrometric measurements [*Cassignol and Gillot*, 1982]. When compared to the $^{40}Ar/^{39}Ar$ method, this alternative method of conventional K-Ar dating has proven successful in dating very young typically subaerial rocks [*Guillou et al.*, 1998; *Ackert et al.*, 2003; *Singer et al.*, 2004; *Guillou et al.*, 2004].

[14] The determination of K was carried out by atomic absorption with a relative precision of 1%. Argon was extracted by radio frequency heating of 0.4 to 1.8 g of sample, then transferred to an ultrahigh-vacuum glass line and purified with titanium sponge and Zr-Ar getters. The analyzed gases must be as pure as possible because active gases present in the mass spectrometer may react with the source filament and therefore change the ionization conditions. Helium, which can penetrate into the line when heating the titanium sponge, is eliminated via cryogenic pumping just before the introduction of the gases into the mass spectrometer. The atmospheric correction is monitored via two separate measurements of atmospheric Ar for each sample. A first atmospheric Ar aliquot (Air-1: reference dose) is measured at the same gas pressure as the sample, and serves as an isotopic reference for the determination of its radiogenic content under identical mass discrimination conditions. The second (Air-2: calibration dose) consists in a manometrically calibrated dose of atmospheric Ar (from a separate reservoir of known ^{40}Ar content). This is used to convert beam intensities into atomic abundances. As both reference aliquots (isotopic and manometric) are atmospheric in composition, they provide a cross check on the radiogenic composition of the sample. Periodic cross calibration of zero-age standards precisely constrains the mass discrimination to within 0.05‰ on the $^{40}Ar/^{36}Ar$ ratios [*Scaillet and Guillou*, 2004].

[15] The manometric calibration of the Air-2 reference is based on repeated determinations of international dating standards of known K-Ar age using the same procedure for the samples to be analyzed as described by *Charbit et al.* [1998]. The total ^{40}Ar content of the sample is determined with a precision of about ±0.2% (2σ). Standards used include LP-6 (127.8 ± 0.7 Ma) [*Odin*, 1982] and HD-B1 (24.21 ± 0.32 Ma) [*Fuhrmann et al.*, 1987; *Hess and Lippolt*, 1994; *Hautmann and Lippolt*, 2000]. At the 95% confidence level, the values adopted here are consistent with those obtained for several $^{40}Ar/^{39}Ar$ standards through the intercalibration against biotite GA-1550 by *Renne et al.* [1998] and *Spell and McDougall* [2003].

[16] In principle, the most critical uncertainty in the K-Ar method is that it is not possible to verify the isotopic composition of the initial argon in the sample. That is, we cannot check the assumption that, at its time of formation, its $^{40}Ar/^{36}Ar$ ratio was the modern atmospheric value (295.5). As a result, the analytical errors given in Table 3 may in principle be less than the real error.

3.2. Results

[17] Age determinations of the PLURIEL samples are reported in Table 3 and on Figure 2. Analysis of each

Table 3. K-Ar Ages of the Selected Samples of the Chain and Plateau Given With a 95% Confidence Level[a]

Sample Ar Experiment	Whole Rock K_2O (wt %)	Whole Rock Nb (ppm)	LOI (%)	K*(wt %)	Weight Molten (g)	40_{Ar}* (%)	$^{40}Ar^{*b}$ (10^{-12} moles/g)	$^{40}Ar^{*c}$ (10^{-12} moles/g)	Age Mean Value[d] (Ma)
DR 14-1-1 7833	*1.76*	*57.6*	*3.44*	*0.664 ± 0.007*	*0.92175*	*36.300*	*9.937 ± 0.051*		
7847				*0.664 ± 0.007*	*0.98453*	*28.741*	*9.419 ± 0.048*	*9.664 ± 0.035*	*8.37 ± 0.18*
DR 24-1-1 7856	0 0.19	4.78	0.29	0.149 ± 0.002	1.05633	17.618	1.431 ± 0.014		
7880				0.149 ± 0.002	0.71068	16.488	1.449 ± 0.015	1.439 ± 0.010	5.56 ± 0.14
DR 8-1-1 7780	0.39	17.6	0.97	0.183 ± 0.002	0.59650	8.685	1.429 ± 0.024		
7797				0.183 ± 0.002	1.77616	13.496	1.406 ± 0.009	1.409 ± 0.008	4.43 ± 0.10
DR 10-2-2 7782	0.37	9.80	0.28	0.183 ± 0.002	0.72771	10.671	1.174 ± 0.019		
7799				0.183 ± 0.002	1.72055	10.992	1.163 ± 0.009	1.165 ± 0.008	3.67 ± 0.09
DR 10-1-1 7885	0.42	8.27	0.25	0.291 ± 0.003	1.24193	7.075	1.533 ± 0.014		
7901				0.291 ± 0.003	0.94859	6.791	1.525 ± 0.015	1.529 ± 0.010	3.03 ± 0.07
DR 34-1-1 7675	0.81	24.7	0.56	0.631 ± 0.006	1.16145	8.848	2.920 ± 0.020		
7691				0.631 ± 0.006	1.00776	9.702	2.870 ± 0.019	2.894 ± 0.014	2.64 ± 0.06
DR 15-2-3 7687	*1.81*	*70.7*	*0.69*	*1.619 ± 0.016*	*0.49595*	*15.835*	*5.909 ± 0.034*		
7703				*1.619 ± 0.016*	*0.43202*	*17.846*	*5.754 ± 0.033*	*5.831 ± 0.023*	*2.08 ± 0.04*
DR 28-1-1 7717	0.12	2.64	0.02	0.075 ± 0.001	1.64586	2.977	0.248 ± 0.008		
7732				0.075 ± 0.001	1.71827	2.841	0.240 ± 0.007	0.244 ± 0.005	1.87 ± 0.09
DR 19-2-2 7669	*1.90*	*62.2*	*1.11*	*1.602 ± 0.016*	*1.22852*	*9.361*	*2.886 ± 0.017*		
7685				*1.602 ± 0.016*	*1.01565*	*8.556*	*2.911 ± 0.019*	*2.898 ± 0.013*	*1.04 ± 0.02*
Sample Ar Experiment	Whole Rock K_2O (wt %)	Whole Rock Nb (ppm)	LOI (%)	K*(wt %)	Weight Molten (g)	40_{Ar}* (%)	$^{40}Ar^{*b}$ (10^{-14} moles/g)	$^{40}Ar^{*c}$ (10^{-14} moles/g)	Age Mean Value[d] (ka)
DR 15-1-1 7884	*2.05*	*79.2*	*0.41*	*1.752 ± 0.018*	*1.04925*	*5.310*	*207.78 ± 1.92*		
7900				*1.752 ± 0.018*	*0.73490*	*4.470*	*208.97 ± 2.00*	*208.35 ± 1.387*	*686 ± 15*
DR 39-1-1 7834	0.20	4.3	−0.32	0.166 ± 0.002	0.95800	1.709	15.890 ± 1.00		
7857				0.166 ± 0.002	1.00300	1.416	15.611 ± 1.56	15.810 ± 0.837	549 ± 59
DR 2-1-1 7855	0.54	14.3	−0.35	0.440 ± 0.004	1.05633	0.857	24.853 ± 1.16		
7891				0.440 ± 0.004	1.00686	0.978	21.041 ± 1.39	23.290 ± 0.893	305 ± 24
DR 4-1-3 7865	0.67	29.0	−0.36	0.548 ± 0.006	1.16565	0.245	10.098 ± 1.46		
7881				0.548 ± 0.006	1.20200	0.227	13.761 ± 1.16	12.681 ± 0.909	133 ± 19
DR 30-1-1 7781	*2.09*	*74.1*	*−0.32*	*1.694 ± 0.017*	*0.77183*	*1.612*	*18.974 ± 1.44*		
7809				*1.694 ± 0.017*	*0.46385*	*0.330*	*17.363 ± 2.62*	*18.6018 ± 1.262*	63 ± 9
DR 1-2-4 7670	0.59	28.9	−0.40	0.515 ± 0.005	1.02667	−0.041	-		
7702				0.515 ± 0.005	1.46920	−0.025	-	-	-
DR 22-4-1 7672	0.55	19.7	1.027	0.457 ± 0.005	1.11685	−0.018	-		
7704				0.457 ± 0.005	1.13631	−0.017	-	-	-
DR 6-1-1 7673	1.33	46.4	0.61	0.996 ± 0.010	0.93340	0.237	2.126		
7716				0.996 ± 0.010	1.01350	−0.256	-	-	-
DR 4-1-5 7674	0.62	24.8	−0.32	0.573 ± 0.006	1.01481	−0.177	-		
7690				0.573 ± 0.006	1.01820	−0.060	-	-	-

[a]Age calculations are based on the decay and abundance constants from *Steiger and Jäger* [1977]. Whole rock K_2O (in wt %, ICP-AES measurement), Nb (in ppm, HR-ICP-MS measurement), and LOI are useful to evaluate the degree of alteration (see text for discussion). To facilitate the reading, the CDP samples are in italics.
[b]Standard error is $\pm 1\sigma$.
[c]Weighted mean $\pm 1\sigma$.
[d]Standard error is $\pm 2\sigma$.

sample involved two determinations each of potassium and argon. The potassium concentrations were combined to yield a mean value and its uncertainty. Separate age determinations were made using each of the argon measurements. The resulting ages and their uncertainties were then combined to yield an overall weighted mean estimate of the age of each sample and its uncertainty. Good analytical reproducibility of $^{40}Ar^*$ determination (see Table 3) is observed for all samples including the very young samples.

[18] K-Ar ages are easily offset by alteration in particular, either leaching out K or adding it via recrystallization to secondary (clay) minerals in the submarine basalts. The same processes may also cause a loss in $^{40}Ar^*$ resulting in higher apparent ages. Consequently, each result has to be confronted with geological constraints or by carrying out repeated analyses from the same rock, or even better yet by dredge samples collected from the same seamounts. All dated samples but one (PLU DR24-1-1) have Ar unspiked ages younger than the underlying crust which means they are geologically meaningful. This sample is dated at 5.56 ± 0.14 Ma and according to the magnetic anomalies, it was formed on a 2 Ma old crust. Its K-Ar age is considered geologically meaningless and thus is discarded. As the sample material looked rather clean (LOI of 0.29), the most likely explanation for this overestimated age is an excess of radiogenic $^{40}Ar^*$ in lava which was not totally degassed prior or during eruption. It is also possible to obtain a "too young" age. For unaltered samples with a low LOI, underestimation of K-Ar ages may come from bias in the experimental procedure. To limit this problem, each sample is analyzed twice, for K and Ar, on two completely separated procedures.

[19] No radiogenic $^{40}Ar^*$ was detected in 4 samples (PLU DR 22-4-1, PLU DR 6-1-1, PLU DR 4-1-5, PLU DR 1-2-4) from the south central zone. These samples presumably are very young and define an area between the segment I2 of the

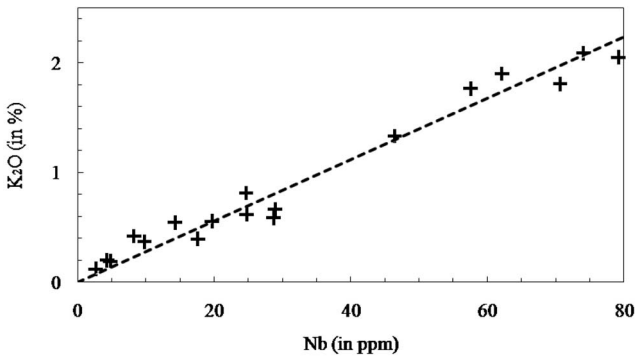

Figure 6. K_2O of the dated samples plotted versus Nb in order to control post magmatic alteration effects. The good correlation ($R^2 = 0.983$) confirms that the samples have not undergone significant post magmatic alteration since alteration would cause increases in K_2O for any Nb value.

SEIR and St. Pierre seamount. According to their K concentration, those samples should be younger than 0.1 Ma. Amsterdam and St. Paul Island as well as Boomerang seamount are located close to this area. Based on paleomagnetic investigations [*Watkins and Nougier*, 1973; *Watkins et al.*, 1975] the building of these islands is considered to be contemporaneous with the Bruhnes period (<780,000 years). St. Paul Island activity has been dated between 20,000 and 40,000 years BP (spiked K-Ar technique [*Watkins et al.*, 1975]) as well as Amsterdam island late activity (Ar/Ar technique [*Carvallo et al.*, 2003]). Boomerang seamount activity is considered to be historical (eruption in 1995, ^{210}Po–^{206}Pb [*Johnson et al.*, 2000]).

4. Discussion

4.1. Origin of the Chain of the Dead Poets

[20] The CDP was regarded as the track of the ASP hot spot on the Australian plate [*Luyendyk and Rennick*, 1977] but our new isotopic ages do not confirm this assumption. M. Maia et al. (submitted manuscript, 2011) calculated with plate kinematic parameters the range of past positions of the ASP hot spot (Figure 3). The hot spot past positions were computed considering a present location centered between Amsterdam and St. Paul islands. The relative movement between the hot spots and the Pacific are from *Gripp and Gordon* [1990] and between the Pacific and Antarctic-Australia from *Cande and Stock* [2004]. They assume that the past positions are probably well constrained between 6 Ma and present. At 6 and 8 Ma the hot spot location is not as precisely constrained as <6 Ma, but a simple hot spot track model predicts that the CDP formed from 14 to 7 Ma. La Fontaine (PLU DR 15), Lamartine (PLU DR 19) and Apollinaire (PLU DR 30) seamounts have K-Ar ages between 2.08 ± 0.04 Ma (PLU DR 15) and 63 +/ 9 ka (PLU DR 30). These ages are much younger than the kinematically modeled ages, so either the K-Ar ages are underestimated or the seamounts are not related to the ASP hot spot activity. As mentioned before, underestimated K-Ar ages cannot be totally excluded due to technical limitations. It seems however very unlikely to systematically underestimate all ages for all the seamounts. We can also exclude systematic datings of late stage activity occurring several My after the main construction of the edifices. Indeed, *Vergara Lopes* [2009] performed a magnetic modeling on the seamounts of the CDP using the method of *Maia et al.* [2005]. The magnetic modeling of the young seamounts reveals that they do not exhibit mixed polarities while the geomagnetic polarity timescale for the last 10 My showed various inversion between normal and reverse polarity [*Cande and Kent*, 1995]. This suggesting that the main stage of construction of the young seamounts occurs within less than 1 My and then that they are formed from a process younger than the ASP hot spot intraplate activity.

[21] Only one seamount, Boileau (PLU DR 14), dated at 8.37 ± 0.18 Ma, fits with the theoretical reconstruction and thus may correspond to the ASP plume activity on the Australian plate. The different phases of activity are summarized on the Figure 8. Its magnetic modeling reveals that Boileau seamount bears a normal magnetization, which is inconsistent with the 8.37 Ma age from our study that must have formed during reversed chron C4r.2r [*Cande and Kent*, 1995]. However, radiometric dating of seamounts is carried out on dredge samples, which are generally biased to a late phase of magmatism. The age of 8.37 Ma obtained for Boileau seamount suggest that the main volcanic phase of its construction occurred during the C4A normal chron, between 8.7 and 9.0 Ma [*Cande and Kent*, 1995].

[22] Boileau seamount age of 8.37 Ma is compatible with the kinematic reconstruction of the ASP hot spot (M. Maia et al., submitted manuscript, 2011) and therefore with an origin directly linked to the hot spot. La Bruyère seamount, large and flat, may be as old as Boileau seamount and related to the ASP hot spot intraplate activity as well. This statement supports the assumption of a possible emerged stage for both of them since they are old enough to have grown above sea level and being eroded subsequently. Conversely, a different origin has to be found for the younger seamounts, which formed when the hot spot already had moved much closer to the current the SEIR. Consequently the CDP as a whole does not correspond to a single hot spot track as describe by *Morgan* [1972].

[23] The CDP therefore results from at least two magmatic events leading to two generations of seamounts. The cause of that magmatic event can be either lithospheric, as consequence of a tectonic event, or deeper, as consequence of a pulse of the hot spot. The CDP exhibits a N65° orientation as well as the CDP seamounts. This elongated shape suggests a tectonic control on the seamounts construction. Boileau and La Bruyère seamounts distinguish from the others because of a larger size and a flat summit. Their larger size may be related to a higher degree of partial melting of the mantle, whereas the other seamounts would have erupted a smaller amount of melts. All the CDP samples are within or close to the tephrite field, regardless of age, which is not consistent with variations in the degree of partial melting through time. However, we cannot totally exclude such variations but it is likely that a longer period of activity and seamount construction should have generated the larger size of Boileau and La Bruyère seamounts.

[24] We note that Apollinaire, Lamartine and La Fontaine seamounts are much younger (0.063–2.08 Ma) than Boileau seamount. Consequently, we assume that the small sharper seamounts Chateaubriand, Sand, and Voltaire, sharing

similar morphological characteristics may belong to this younger group.

[25] All the seamounts have a N65° orientation, which means that despites their different sizes they share some morphological characteristics. This is suggesting that a common tectonic event occurred at about 8 Ma (with Boileau construction) and lasted since 2 Ma (with the young seamounts construction). The magnetic modeling of the seamounts [*Vergara Lopes*, 2009] revealed that five seamounts exhibit a normal polarity and two are mixes of normal and reverse polarities. The mixed polarity of the geomagnetic polarity timescale for the last 10 My showed various inversion and a 1:1 repartition between normal and reverse polarity. This disagrees with the bias toward normal polarities recording the CDP seamounts suggesting that the construction of the CDP was not a continuous process. The two generations would then correspond to two "events" and not to a bias of sampling. M. Maia et al. (submitted manuscript, 2011) showed that ASP plume activity has not been regular but with pulses of higher magmatic activity and separated by a more or less quiet period. These two pulses have been recorded in the morphology of the ASP plateau and took place from 10 to 6 Ma ago and for the last 3 Ma. It is likely that the higher flux of material from the ASP plume extended laterally and ponded some material during the early stage of the plateau formation, leading to the construction of Boileau seamount. When a ridge and a plume come together most of the magmatism is driven toward the ridge melting zone but some of it can also be driven to the surface along stressed areas in the lithosphere. This area being in extension, a plume pulse can induce the construction of volcanoes away from the plateau, where the lithosphere is thinner and fragile. This process is related to the plume pulse and so it is expected to have occurred during the two periods of high magmatic production. This implies that the construction of the young seamounts should have occurred since 3 Ma, even if we collected no samples older than 2.08 ± 0.04 Ma. The hot spot pulses induced the construction of the two generations of seamounts with a partial tectonic control so the maximum extension between Capricorn and Australian plates should be orthogonal to the associated volcanoes. Therefore, the N65° orientation of the chain and the seamounts constrains the maximum divergence as N155°. As there is no difference in the orientation of old and young seamounts, there seems to be no significant variation of direction of divergence between the Capricorn and Australian plates for the last 8 Ma.

[26] La Fontaine seamount is the only seamount that does not show an elongation. It is segmented from the other seamounts by the SPFZ, which offsets magnetic lineation about 10 My. Consequently, La Fontaine seamount is located on lithosphere 10 My older than that which underlies Lamartine, Apollinaire, and other seamounts. A 10 My older lithosphere is thicker and more robust and so may be less susceptible to deformations.

[27] In summary, the timing and morphology of the seamounts is controlled both by the ASP plume activity and the regional lithospheric stresses induced by the plate motions. In addition, the plume pulses could act mechanically on the lithosphere to increase deformation and cause volcanic activity on the surface. This could especially be realistic for the 10–6 Ma ASP hot spot pulse since the plume was closest to a deformed area. In fact, the source of the magmatism (ASP plume) was 400 km closer to the deformations field when Boileau and La Bruyère seamounts formed compared to the phase in which the younger seamounts were formed. Consequently, the amount of ponded plume material reaching the chain location would be higher for similar pulse intensity and would thus result in the construction of larger edifices.

[28] The lithosphere was much older and thicker during the construction of the young seamounts than for the old ones (12 My old lithosphere against 7 My). This would have forced a deeper mantle melting which is consistent with the lower partial melting observed for the young seamounts. In conclusion, we assume that the old seamounts are larger because they formed closer to the hot spot through a greater degree of partial melting of the mantle over a lithosphere that was more stressed and thus allowed for an easier pathway of the seamount magmas.

4.2. The ASP Plateau as a Product of the ASP Plume-SEIR Interaction

[29] From the previous discussion we understand that magmatic activity has changed during the construction of ASP plateau as follows: (1) the first on-axis phase occurred when the SEIR and hot spot melting regions were connected resulting in the formation of the axial plateau and (2) a second off-axis phase produced small volcanoes on the Australian plate in the northern part of ASP plateau. On- and off-axis samples are primarily tholeiitic basalt, as well as Amsterdam and St. Paul islands, which contrasts with the alkaline lavas recovered from the CDP (Figure 5). On- and off-axis samples thus derive from common (or similar) sources and processes. Our radiogenic ages compared with the calculated position of the hot spot in the past (see M. Maia et al., submitted manuscript, 2011) and to the evolution of the SEIR axis position (E. Courreges et al., submitted manuscript, 2011) allow us to describe the evolution of the geodynamical surrounding when on- and off-axis magmatic activity occurred.

[30] PLU DR 8-1-1, PLU DR 10-1-1, PLU DR 10-2-2, PLU DR 28-1-1, and PLU DR39-1-1 are dated samples representing the off-axis activity of the plateau. We plotted the K-Ar ages of the off-axis volcanism samples (onto and outside the plateau) (y, in My) versus the current position of the ASP plume (between Amsterdam and St. Paul islands) (x, in km) [*Royer and Schlich*, 1988] (Figure 7a). With the exception of Rimbaud seamount (PLU DR 39), located on Amsterdam fracture zone, all the ages of the plateau systematically increase with the distance from Amsterdam and St. Paul islands. Rimbaud seamount is located on Amsterdam FZ and is clearly bigger than the others seamounts located on the same FZ. Its construction occurred on a weak area, during a plume pulse period so it is likely that its construction have been influenced by tectonic settings contrary to the other off-axis volcanoes located between fractures zones. Consequently, we excluded it from the discussion hereafter.

[31] We applied a level headedness to the ages according to their distance from the plume to avoid bias toward the current hot spot activity. A linear correlation is observed, which equation is $y = 0.0107\ x$ for a correlation factor $R^2 = 0.963$. This linearity corresponds to the motion of the

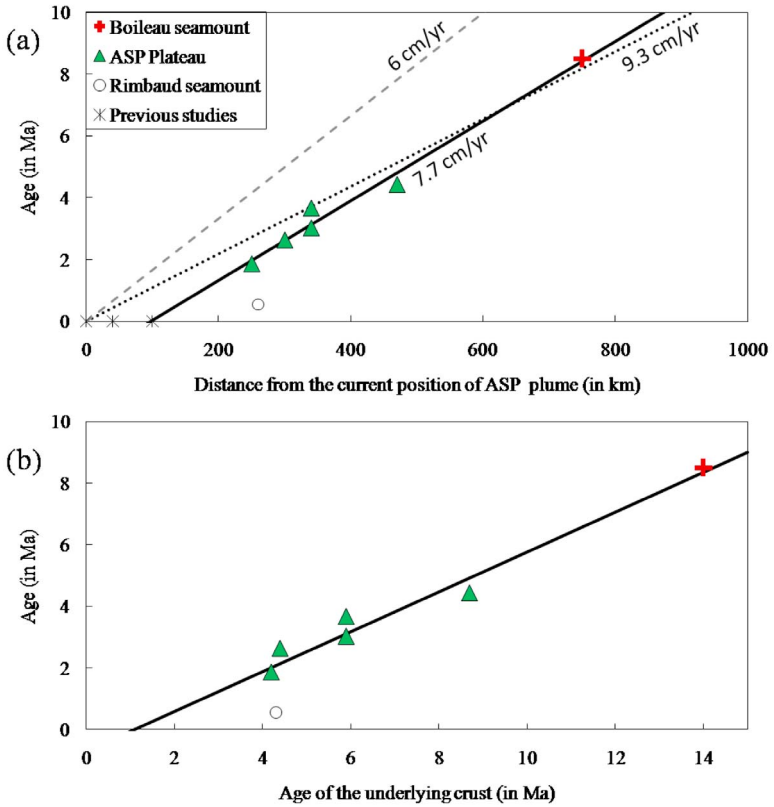

Figure 7. (a) Distance from the current position of ASP plume (in km) versus K-Ar ages (in Ma) of samples related to ASP plume activity. The previous studies samples are Amsterdam and St. Paul islands and Boomerang seamount [*Watkins et al.*, 1975; *Carvallo et al.*, 2003; *Johnson et al.*, 2000]. Dotted black line corresponds to the correlation equation y = 0.0107 x for a correlation factor R^2 = 0.963. The calculated velocity of the Capricorn-Australian block is about 9.3 cm/yr. If we consider the samples related to ASP plume activity only on the Australian plate (see text for discussion), the correlation equation becomes y = 0.0129 x −1.249 for a correlation factor R^2 = 0.988 (solid black line). The calculated velocity is about 7.7 cm/yr (see text for discussion), requiring ASP plume velocity consistent with other hot spot motions. (b) K-Ar dating of off-axis magmatism plotted versus the age of the underlying crust (obtained from magnetic data). The samples used are from ASP plateau and from Boileau seamount. The correlation equation is 0.054 x −1.298 for a correlation factor R^2 = 0.823. The associated convergence between ASP plume and the SEIR is inconsistent with a straight motion of the SEIR. This discrepancy confirms the SEIR jump to the SW evidenced by M. Maia et al. (submitted manuscript, 2011).

Capricorn and Australian plates considering they are moving together toward the NE. The calculated motion of the Capricorn-Australian block is of 9.3 cm/yr to the NE in a fixed plume model [*Morgan*, 1972]. The SEIR is a ridge of intermediate spreading rate [*Sempéré and Cochran*, 1997; *Conder and Forsyth*, 2000], which on the I2 segment has an average of 5.94 cm/yr for the last 10 My (E. Courreges et al., submitted manuscript, 2011). With a fixed Antarctic plate, this spreading rate concurs totally to the SEIR and the Capricorn-Australian block motions. Consequently, the apparent 9.3 cm/yr motion of the Capricorn-Australian block calculated with respect to a fixed ASP plume is too rapid to be due only to the spreading of the SEIR axis with a half-spreading rate of 2.97 cm/yr. Indeed, a motion of the Capricorn-Australian block only due to the SEIR spreading would be less than 6 cm/yr. This velocity corresponds to a slope of 1/60 = 0.017; no edifices lie on this line (Figure 7a). One explanation for this discrepancy could be that the ASP plume is not fixed. In that case, the absolute motion of the plume would be of about 3–4 cm/yr to the SW. However, this velocity is inconsistent with other hot spot motions like Hawaiian hot spot, which has been moving with a velocity of 1 cm/yr for the last 10 My [*Kono*, 1980; *Tarduno et al.*, 2003; *Duncan et al.*, 2006] as well as Indian Ocean hot spots [*O'Neill et al.*, 2003]. This overestimation results from the discrepancy between samples from off-axis edifices built on a fixed Antarctic plate and on a moving Capricorn-Australian. The deflection of the plume induced by the plate motions is thus different between the two sets of samples. If we remove all the ages of Antarctic plate edifices, the correlation becomes y = 0.0129 x −1.249 for a correlation factor R^2 = 0.988 (Figure 7b). The nonzero intercept translate the deflection of the plume toward the NE in response to the overlying plate movement, when compared

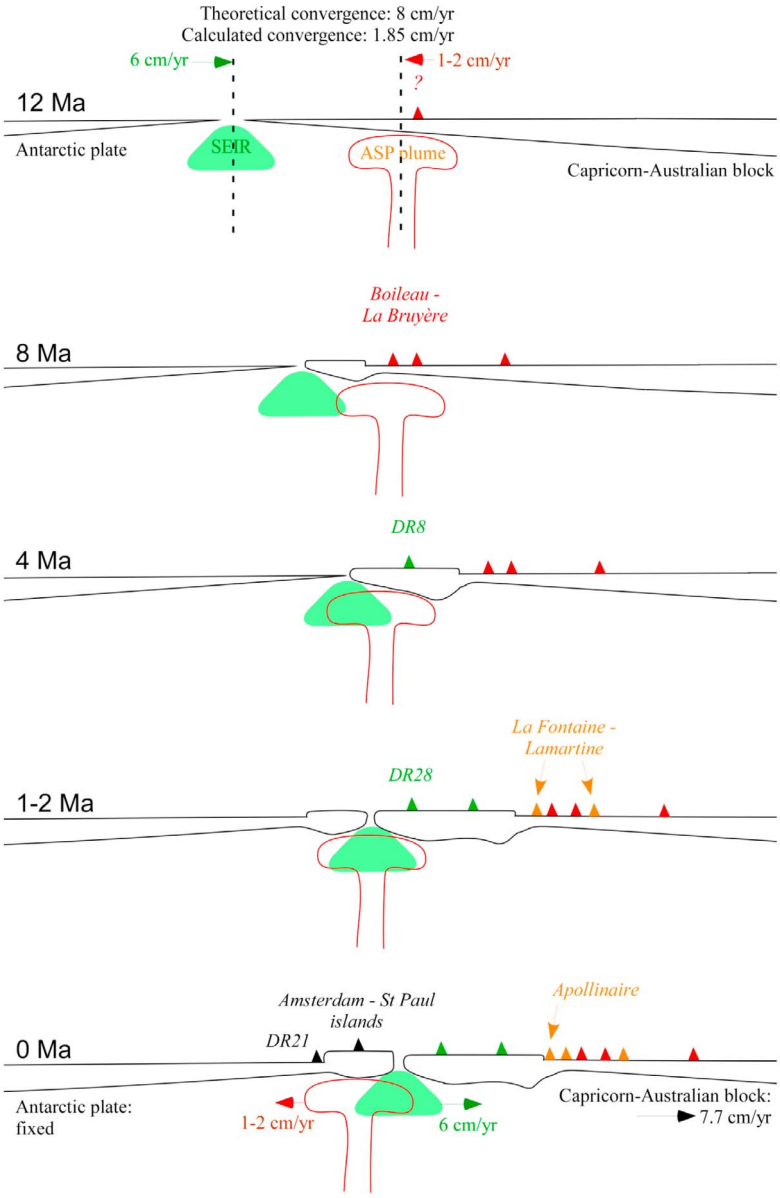

Figure 8. Successive schematic cross sections through the ASP plateau and the chain of Dead Poets showing the different periods of magmatism through time and the calculated motions. The position of ASP plume is based on the paleopositions modeled by M. Maia et al. (submitted manuscript, 2011). The first phase at 12 My is purely speculative but indicates that there are no arguments to exclude a volcanism before the construction of Boileau seamount.

to a centered plume activity. The off-axis edifices of the Capricorn-Australian plate are thus shifted of about 100 km (x = 96 km for y = 0) when compared to the position of ASP plume at the time of the eruption. Considering the currently accepted plume "diameters" (150 km) [*Ito et al.*, 1997; *Wolfe et al.*, 2005], and considering that ASP is probably a small hot spot of with a diameter of about 80 km (M. Maia et al., submitted manuscript, 2011), this shift is perfectly understandable and does not affect the slope of the observed correlation between K-Ar ages of the off-axis volcanism samples and the current position of the ASP plume. This correlation thus provides a 7.7 cm/yr motion of the Capricorn-Australian block, which is also too rapid to be due only to the spreading of the SEIR. This correlation thus provides 1–2 cm/yr motion to the SW of ASP plume, which is consistent with other hot spots motions. Therefore, we assume that the ASP plume motion is about 1–2 cm/yr to the SW.

[32] *O'Neill et al.* [2003] calculated the motion of the Indian hot spots employing a plate motion revised and a tomography model to calculate mantle flow through time. They provided modeled motions consistent with the paleolatitutes estimates for the Kerguelen and Réunion hot spot. They also calculated ASP hot spot of the last 120 Ma but could not constraint it with measured paleolatitutes. Their

modeling suggests a motion to north between 120 and 60 Ma and to south at since 60 Ma, with an average velocity of 0.28 cm/yr. Nevertheless, the discrepancy with our conclusions does not exclude any model since their calculations concern a motion though 120 My and ours for that last 10 My. The changing motion at about 60 Ma precludes a constant velocity though time. The average velocity given by *O'Neill et al.* [2003] is thus compatible with our data.

[33] A plot of K-Ar ages versus age of the underlying crust (Figure 7b) provides an estimate of the motion of the SEIR relative to the hot spot. In order to calculate a more precise motion vector, we added a sample from Boileau since it is also related to the off-axis activity of the ASP hot spot. We observe a linear correlation, which equation is $y = 0.648\ x - 0.717$ for a correlation factor $R^2 = 0.976$, with y corresponding to the age of the off-axis volcanoes (in Ma) and x the age of the underlying crust (in Ma). The age of the underlying crust is directly related to the distance from the ridge. Courreges and coworkers suggested that the average half-spreading rate of segment I2 is 2.97 cm/yr during the period of the plateau construction. Using this information, we can convert the age of the underlying crust into the distance from the SEIR at the time of the off-axis volcano construction and plot the off-axis volcanoes (y, in Ma) versus their distance to the SEIR (x, in km). The correlation observed then becomes $y = 0.054\ x - 1.298$ with a correlation factor $R^2 = 0.823$. The inverse of the slope, $1/0.054 = 18.5$ corresponds to the relative motion between the SEIR and ASP plume in km/Ma. In other words, the SEIR and the ASP seem to have converged with a velocity of 1.85 cm/yr. This relative motion is the vectorial sum of the absolute motions of the SEIR itself, the ASP plume and the Indo-Australian plate. All those motions have been reported on the Figure 8 cartoon. Considering the Antarctic plate as fixed, the SEIR moving from SW to NE at 6 cm/yr and the ASP plume moving from NE to SW at 1–2 cm/yr, the relative convergence of 1.85 cm/yr between the SEIR and the plume is too small to be realistic. This means that the motion of the SEIR has not been continuous to the NE during this period. Those results confirm then the SEIR jumps to the SW evidenced by M. Maia et al. (submitted manuscript, 2011).

[34] *Behn et al.* [2004] suggested that a strong asthenospheric flow is moving away from Africa (superswell). In this case, the ridge and the plume would be moving to the East and the apparent motion of the Capricorn-Australian plate versus the hot spot would be lower than the SEIR half-spreading rate creating the I2 plate segment. Conversely, *Steinberger* [2000] calculated the deformation of plumes deep-seated conduit in order to estimate the surface hot spots tracks. He evidenced that plume conduits were tilted toward large upwellings because of the lower mantle flow. In this case, the hot spot surface motion often represents the horizontal component of the midmantle flow, generally opposite to the plate motion. The ASP plume, however, is moving toward the SW. This means that ASP plume has been moving toward the ridge, toward the large African superswell and thus against the asthenospheric flow. This movement thus requires a deep-seated conduit, which suggests that ASP plume origin is located in the lower mantle.

[35] *Zhao* [2007] provides tomographic images under sixty major hot spot, including ASP. They evidence continuous low-velocity anomalies in both upper and lower mantle visible under ASP plateau, suggesting that ASP hot spot could be originating from the core-mantle boundary. This is in agreement with the deep-seated conduit evidenced here. In addition, the tilted images of the so-called ASP plume toward Africa consolidate Steinberger's conclusions and thus ours.

5. Conclusion

[36] This study showed that the ASP hot spot activity and interaction with the SEIR is complex. The geochronological constraints of the various phases of activity allow an evaluation of the relative and absolute motion of the plates and the plume involved in the system.

[37] First, the chain of seamounts considered as the ASP plume intraplate activity is made of two generations of seamounts, related to both ASP plume activity and regional tectonic settings: (1) large edifices were formed between 10 and 8 Ma, which possibly reached the surface as evidenced by their flat summit and (2) smaller edifices were constructed over the past 2–3 My. The ASP plume is a small plume, which expresses onto a weak lithosphere and in a non regular way through time. The construction of the CDP is then due to the conjunction of the plume pulse and of stresses at the Capricorn-Australian diffuse boundary, leading melts toward the surface. The elongated shape of the seamounts of the CDP indicates that the maximum deformation between Australian and Capricorn plates occurred along a N155° direction for the last 10 Ma. The conjunction of plume pulse on a weak lithosphere also induced the construction of volcanic edifices (like Rimbaud seamount) on the ASP plateau.

[38] Second, the apparent velocity of the Capricorn-Australian block northeastward does not fit with a fixed plume model *Morgan* [1972]. We assume that the ASP plume motion is about 1–2 cm/yr to the SW. This motion in the opposite direction of the atshenospheric flow requires deep-seated anchorage of the conduit and so a deep origin for ASP plume.

[39] Finally, the relative convergence calculated between the SEIR and the plume is inconsistent with a continuous movement of the SEIR toward NE for the last 10 My, confirming then the SEIR jumps to the SW evidenced by M. Maia et al. (submitted manuscript, 2011) during this period.

[40] **Acknowledgments.** We thank Captain Duchesne, the crew of the *Marion Dufresne II*, and the PLURIEL scientific party for their help with the acquisition and treatment of the data. This manuscript benefited from constructive comments from A. Hofmann and J. Dyment. We are also indebted to F. Frey and A. Koppers, who helped improve the manuscript. The PLURIEL cruise was funded by the Centre National de la Recherche Scientifique–Institut Nationale des Sciences de l'Univers through the program SEDIT, by IPEV, and by the program EXTRAPLAC.

References

Ackert, R. P., B. Singer, H. Guillou, M. R. Kaplan, and M. D. Kurz (2003), Long-term cosmogenic ^{3}He production rates from ^{40}Ar/^{39}Ar and K-Ar dated Patagonian lava flows at 47°S, *Earth Planet. Sci. Lett.*, *210*, 119–136, doi:10.1016/S0012-821X(03)00134-1.

Behn, M. D., C. P. Conrad, and P. G. Silver (2004), Detection of upper mantle flow associated with the African superplume, *Earth Planet. Sci. Lett.*, *224*, 259–274, doi:10.1016/j.epsl.2004.05.026.

Cande, S. C., and D. V. Kent (1995), Revised calibration of the geomagnetic polarity timescale for the Late Cretaceous and Cenozoic, *J. Geophys. Res.*, *100*, 6093–6095, doi:10.1029/94JB03098.

Cande, S. C., and J. Stock (2004), Cenozoic reconstructions of the Australia-New Zealand-South Pacific sector of Antarctica, in *The Cenozoic Southern Ocean: Tectonics, Sedimentation and Climate Change Between Australia and Antarctica*, *Geophys. Monagr. Ser.*, vol. 151, edited by N. Exon, J. K. Kenett, and M. Malone, pp. 5–17, AGU, Washington, D. C.

Carvallo, C., P. Camps, G. Ruffet, B. Henry, and T. Poidras (2003), Mono Lake or Laschamp geomagnetic event recorded from lava flows in Amsterdam Island (southeastern Indian Ocean), *Geophys. J. Int.*, *154*, 767–782, doi:10.1046/j.1365-246X.2003.01993.x.

Cassignol, C., and P. Y. Gillot (1982), Range and effectiveness of unspiked potassium-argon dating: Experimental groundwork and applications, in *Numerical Dating in Stratigraphy*, edited by G. S. Odin, pp. 159–179, John Wiley, Chichester, U. K.

Charbit, S., H. Guillou, and L. Turpin (1998), Cross calibration of K-Ar standard minerals using unspiked Ar measurement technique, *Chem. Geol.*, *150*, 147–159, doi:10.1016/S0009-2541(98)00049-7.

Conder, J. A., and D. W. Forsyth (2001), Seafloor spreading on the Southeast Indian Ridge over the last one million years: A test of the Capricorn plate hypothesis, *Earth Planet. Sci. Lett.*, *188*, 91–105, doi:10.1016/S0012-821X(01)00326-0.

Dalrymple, G. B., and M. A. Lanphere (1968), *Potassium-Argon dating: Principles Techniques and Applications to Geochronology*, 251 pp., W.H. Freeman, San Francisco, Calif.

Demets, C., R. G. Gordon, and D. F. Argus (1988), Intraplate deformation and closure of the Australia-Antarctica-Africa plate circuit, *J. Geophys. Res.*, *93*, 11,877–11,897, doi:10.1029/JB093iB10p11877.

Demets, C., R. G. Gordon, and P. Vogt (1994), Location of the Africa-Australia-India triple junction and motion between the Australian and Indian Plates: Results from an aeromagnetic investigation of the central Indian and Carlsberg ridges, *Geophys. J. Int.*, *119*, 893–930, doi:10.1111/j.1365-246X.1994.tb04025.x.

Doucet, S., D. Weis, J. S. Scoates, V. Debaille, and A. Giret (2004), Geochemical and Hf-Pb-Sr-Nd isotopic constraints on the origin of the Amsterdam–St. Paul (Indian Ocean) hot spot basalts, *Earth Planet. Sci. Lett.*, *218*, 179–195, doi:10.1016/S0012-821X(03)00636-8.

Duncan, R. A., and L. G. Hogan (1994), Radiometric dating of young MORB using the $^{40}Ar/^{39}Ar$ incremental heating method, *Geophys. Res. Lett.*, *21*, 1927–1930, doi:10.1029/94GL01375.

Duncan, R. A., J. A. Tarduno, and D. W. Scholl (2006), Leg 197 synthesis: Southward motion and geochemical variability of the Hawaiian hot spot, *Proc. Ocean Drill. Program, Sci. Results*, *197*, 1–39.

Frey, F. A., D. Weis, H.-J. Yang, K. Nicolaysen, H. Leyrit, and A. Giret (2000), Temporal geochemical trends in Kerguelen Archipelago basalts: Evidence for decreasing magma supply from the Kerguelen plume, *Chem. Geol.*, *164*, 61–80.

Fuhrmann, U., H. Lippolt, and C. J. Hess (1987), HD-B1 biotite reference material for K-Ar chronometry, *Chem. Geol.*, *66*, 41–51.

Gente, P., J. Dyment, M. Maia, and J. Goslin (2003), Interaction between the Mid-Atlantic Ridge and the Azores hot spot during the last 85 Myr: Emplacement and rifting of the hot spot-derived plateaus, *Geochem. Geophys. Geosyst.*, *4*(10), 8514, doi:10.1029/2003GC000527.

Gripp, A. E., and R. G. Gordon (1990), Current plate velocities relative to the hot spots incorporating the NUVEL-1 global plate motion model, *Geophys. Res. Lett.*, *17*, 1109–1112, doi:10.1029/GL017i008p01109.

Guillou, H., J. C. Carracedo, and S. Day (1998), Dating the upper Pleistocene-Holocene volcanic activity of La Palma using the unspiked K-Ar technique, *J. Volcanol. Geotherm. Res.*, *86*, 137–149, doi:10.1016/S0377-0273(98)00074-2.

Guillou, H., B. Singer, C. Laj, C. Kissel, S. Scaillet, and B. R. Jicha (2004), On the age of the Laschamp geomagnetic event, *Earth Planet. Sci. Lett.*, *227*, 331–343, doi:10.1016/j.epsl.2004.09.018.

Hautmann, H. J., and H. Lippolt (2000), $^{40}Ar/^{39}Ar$ dating of central European K-Mn oxides: A chronological frameworkof supergene alteration processes during the Neogene, *Chem. Geol.*, *170*, 37–80, doi:10.1016/S0009-2541(99)00241-7.

Hess, C. J., and H. Lippolt (1994), Compilation of K-Ar measurements on HD-B1 standard biotite, in *Phanerozoic Time Scale*, edited by G. S. Odin, *Bull. Liais. Inform.*, *12*, 19–23.

Ito, G., J. Lin, and C. W. Gable (1997), Interaction of mantle plumes and migrating mid-ocean ridges: Implications for the Galapagos plume-ridge system, *J. Geophys. Res.*, *102*, 15,403–15,417.

Johnson, K. T. M., D. W. Graham, K. H. Rubin, K. Nicolaysen, D. S. Scheirer, D. W. Forsyth, E. T. Baker, and L. M. Douglas-Priebe (2000), Boomerang Seamount: The active expression of the Amsterdam–St. Paul hot spot, Southeast Indian Ridge, *Earth Planet. Sci. Lett.*, *183*, 245–259, doi:10.1016/S0012-821X(00)00279-X.

Kono, M. (1980), Paleomagnetism of DSDP Leg 55 basalts and implications for the tectonics of the Pacific Plate, *Initial Rep. Deep Sea Drill. Proj.*, *55*, 737–752.

Le Bas, M. J., R. W. Le Maitre, and A. R. Woolley (1992), The construction of the Toral Alkali-Silica chemical classification of volcanic rocks, *Mineral. Petrol.*, *46*(1), 1–22, doi:10.1007/BF01160698.

Luyendyk, B. P., and W. Rennick (1977), Tectonic history of aseismic ridges in the eastern Indian Ocean, *Geol. Soc. Am. Bull.*, *88*, 1347–1356, doi:10.1130/0016-7606(1977)88<1347:THOARI>2.0.CO;2.

Maia, M., J. Dyment, and D. Jouannetaud (2005), Constraints on age and construction process of the foundation chain submarine volcanoes from magnetic modeling, *Earth Planet. Sci. Lett.*, *235*, 183–199, doi:10.1016/j.epsl.2005.02.044.

Maia, M., et al. (2008), Evolution of the Saint Paul Amsterdam plateau in the last 10 m.y., *Eos Trans. AGU*, *89*(53), Fall Meet. Suppl., Abstract T54B–06.

Minster, J., and T. Jordan (1978), Present-day plate motions, *J. Geophys. Res.*, *83*, 5331–5354, doi:10.1029/JB083iB11p05331.

Morgan, W. J. (1972), Deep mantle convection plumes and plate motions, *Am. Assoc. Pet. Geol. Bull.*, *56*, 203–213.

Nicolaysen, K. P., F. A. Frey, J. J. Mahoney, K. T. M. Johnson, and D. W. Graham (2007), Influence of the Amsterdam/St. Paul hot spot along the Southeast Indian Ridge between 77° and 88°E: Correlations of Sr, Nd, Pb and He isotopic variations with ridge segmentation, *Geochem. Geophys. Geosyst.*, *8*, Q09007, doi:10.1029/2006GC001540.

Odin, G. S. (1982), Interlaboratory standards for dating purposes, in *Numerical Dating in Stratigraphy*, edited by G. S. Odin, pp. 123–150, John Wiley, Chichester, U. K.

O'Neill, C., D. Müller, and B. Steinberger (2003), Geodynamic implications of moving Indian Ocean hot spots, *Earth Planet. Sci. Lett.*, *215*, 151–168, doi:10.1016/S0012-821X(03)00368-6.

Renne, P. R., C. C. Swisher, A. L. Deino, D. B. Karner, T. L. Owen, and D. J. DePaolo (1998), Intercalibration of standards, absolute ages and uncertainties in $^{40}Ar/^{39}Ar$ dating, *Chem. Geol.*, *145*, 117–152, doi:10.1016/S0009-2541(97)00159-9.

Royer, J. Y., and R. G. Gordon (1997), The motion and boundary between the Capricorn and the Australian plates, *Science*, *277*, 1268–1274, doi:10.1126/science.277.5330.1268.

Royer, J. Y., and R. Schlich (1988), Southeast Indian Ridge between the Rodriguez Triple Junction and the Amsterdam and St. Paul islands: Detailed kinematics for the past 20 m.y., *J. Geophys. Res.*, *93*, 13,524–13,550, doi:10.1029/JB093iB11p13524.

Scaillet, S., and H. Guillou (2004), A critical evaluation of young (near-zero) K-Ar ages, *Earth Planet. Sci. Lett.*, *220*, 265–275, doi:10.1016/S0012-821X(04)00069-X.

Schilling, J.-G. (1973), Iceland mantle plume: Geochemical study of Reykjanes ridge, *Nature*, *242*, 565–571, doi:10.1038/242565a0.

Schilling, J.-G. (1991), Fluxes and excess temperatures of mantle plumes inferred from their interaction with migrating mid-ocean ridges, *Nature*, *352*, 397–403, doi:10.1038/352397a0.

Sempéré, J. C., and J. R. Cochran (1997), The Southeast Indian Ridge between 88°E and 118°E: Variations in crustal accretion at constant spreading rate, *J. Geophys. Res.*, *102*, 15,489–15,505, doi:10.1029/97JB00171.

Singer, B. S., R. P. Ackert, and H. Guillou (2004), $^{40}Ar/^{39}Ar$ and K-Ar geochronology of Pleistocene glaciations in Patagonia, *Geol. Soc. Am. Bull.*, *116*, 434–450, doi:10.1130/B25177.1.

Spell, T. L., and I. McDougall (2003), Characterization and calibration of $^{40}Ar/^{39}Ar$ dating standards, *Chem. Geol.*, *198*, 189–211, doi:10.1016/S0009-2541(03)00005-6.

Steiger, R. H., and E. Jäger (1977), Subcommission on geochronology: Convention of the use of decay constants in geo and cosmochronology, *Earth Planet. Sci. Lett.*, *36*, 359–362, doi:10.1016/0012-821X(77)90060-7.

Stein, S., and R. G. Gordon (1984), Statistical tests of additional plate boundaries from plate motion invertions, *Earth Planet. Sci. Lett.*, *69*, 401–412, doi:10.1016/0012-821X(84)90198-5.

Steinberger, B. (2000), Plumes in a convecting mantle: Models and observations from individual hot spots, *J. Geophys. Res.*, *105*, 11,127–11,152.

Tarduno, J. A., et al. (2003), The Emperor Seamounts: Southward motion of the Hawaiian hot spot plume in Earth's mantle, *Science*, *301*, 1064–1069, doi:10.1126/science.1086442.

Vergara Lopes, P. (2009), Modelagem magnetic dos vulcoes do alinhemento dos Poetas Desaparecidos, M.S. dissertation, Univ. Fed. Fluminense, Rio de Janeiro, Brazil.

Vogt, P. R. (1976), Plumes, subaxial pipe flow and topography along the mid-oceanic ridge, *Earth Planet. Sci. Lett.*, *29*, 309–325, doi:10.1016/0012-821X(76)90135-7.

Watkins, N. D., and J. Nougier (1973), Excursions and secular variation of the Bruhnes epoch geomagnetic field in the Indian Ocean region, *J. Geophys. Res.*, *78*, 6060–6068, doi:10.1029/JB078i026p06060.

Watkins, N. D., I. McDougall, and J. Nougier (1975), Paleomagnetism and potassium-argon age of St. Paul Island, southeastern Indian Ocean: Contrasts in geomagnetic secular variation during the Brunhes Epoch, *Earth Planet. Sci. Lett.*, *24*, 377–384, doi:10.1016/0012-821X(75)90144-2.

Wiens, D. A., et al. (1985), A diffuse plate boundary model for Indian Ocean tectonics, *Geophys. Res. Lett.*, *12*, 429–432, doi:10.1029/GL012i007p00429.

Wolfe, J. A., M. C. Rowe, R. Teasdale, J. N. Gardner, F. C. Ramos, and C. E. Heikoop (2005), Petrogenesis of pre-caldera mafic lavas, Jemez mountains volcanic field (New Mexico, USA), *J. Petrol.*, *46*, 407–439.

Zhao, D. (2007), Seismic images under 60 hot spots: Search for mantle plumes, *Gondwana Res.*, *12*, 335–355, doi:10.1016/j.gr.2007.03.001.

C. Bollinger, C. Hémond, M. Janin, C. Liorzou, and M. Maia, Domaines Océaniques, Océaniques, UMR 6538, Université de Brest, CNRS, Institut Universitaire Européen de la Mer, Place Copernic, F-29280 Plouzané, France.

H. Guillou, LSCE/IPSL, Laboratoire CEA-CNRS-UVSQ Domaine du CNRS, Bât. 12, Ave. de la Terrasse, F-91198 Gif sur Yvette, France.

K. T. M. Johnson, School of Ocean and Earth Science and Technology, University of Hawaii, Honolulu, HI 96822, USA.

A. Mudholkar, National Institute of Oceanography, Dona Paula, Goa, 403004, India.